Chapter 4

Results and Discussion

4.4 Simulation of DC Glow Discharge

4.1.1 Electrical characteristics

Several experimental studies on DC glow discharges have been carried out in the Plasma Research Laboratory prior to as well as during the current simulation study. The DC glow discharge setup used in a recent study by Safaai [3] is shown schematically in Figure 4.1.

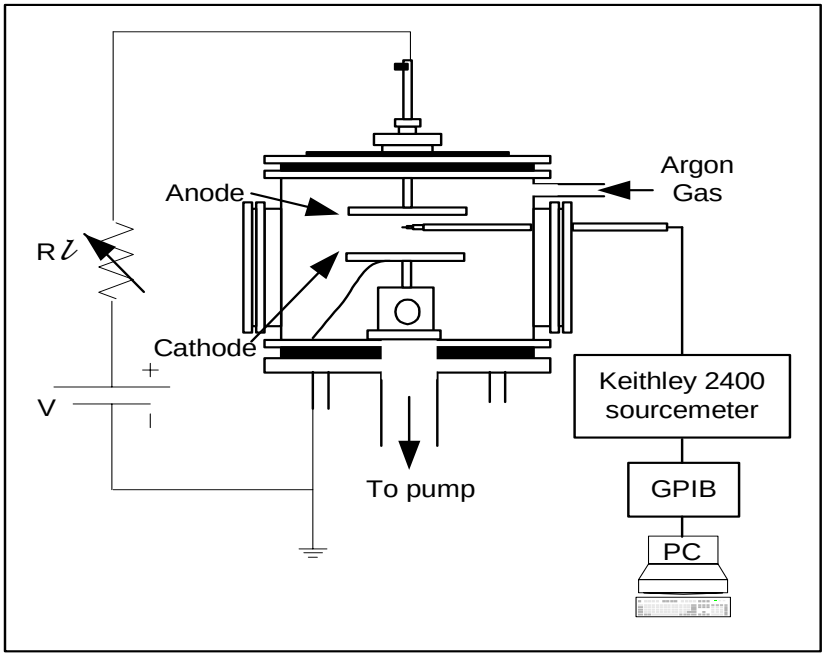

Figure 4.1: Schematic experimental setup of the DC glow discharge system [3].

The electrode separation was varied from 3 cm to 7 cm, with copper parallel plate electrode of diameter 6.5 cm. The filling gas was argon, and the discharge was operated at a pressure in the range of 0.75 to 3 Torr (1 to 4 mbar). The discharge characteristics were studied by measuring the *I-V* characteristics of the discharge from which the operating condition for normal glow discharge was determined. An example of the results obtained is shown in Figure 4.2. The DC power supply was set at an output voltage in the range of 300 - 500 V. It can be seen that for the experimental setup with electrode separation of 3 cm and argon pressure of 4 mbar, a normal glow discharge is obtained when the discharge current is maintained in the range of about 5 to 32 mA, where the voltage across the electrodes remains constant at about 200 V. When the pressure is reduced to 2.5 mbar, the anode potential shifted to a higher value of about 225 V within the same range of discharge current. For an electrode separation of 5 cm, the anode potential was measured to be at about 225 V for pressure of 4 mbar and 2.5 mbar at normal glow discharge operation at discharge current in the range of 5 to 32 mA. This is also the case for electrode separation of 2.5 mbar. However, for all three electrode separations tested, the argon glow discharge obtained is abnormal even at discharge current below 5 mA when the operating pressure is 1 mbar or lower.

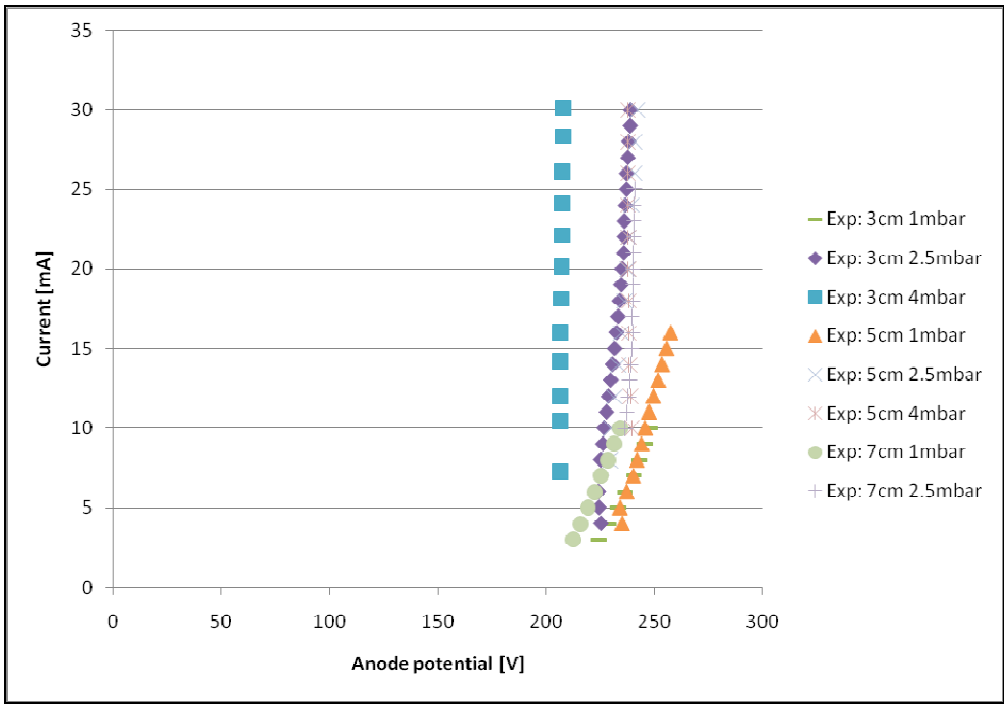

Figure 4.2: Experimental I-V characteristics of DC glow discharge.

The potential distribution across the electrodes for the normal glow discharge obtained at conditions of 3 cm electrode separation and 4 mbar operating pressure has also been measured as shown in Figure 4.3, while the corresponding electric field can be deduced from this graphs and plotted together. The potential as well as electric field distributions across the electrodes are those as expected for a normal glow discharge. The potential drops from the value of about 200 V across a cathode fall region with thickness of about 5 mm to the ground potential at the cathode surface. Correspondingly, the electric field is seen to be highest at the cathode surface, with a value of about 2.5 kV/cm which drops to near zero across the 5 mm cathode fall region.

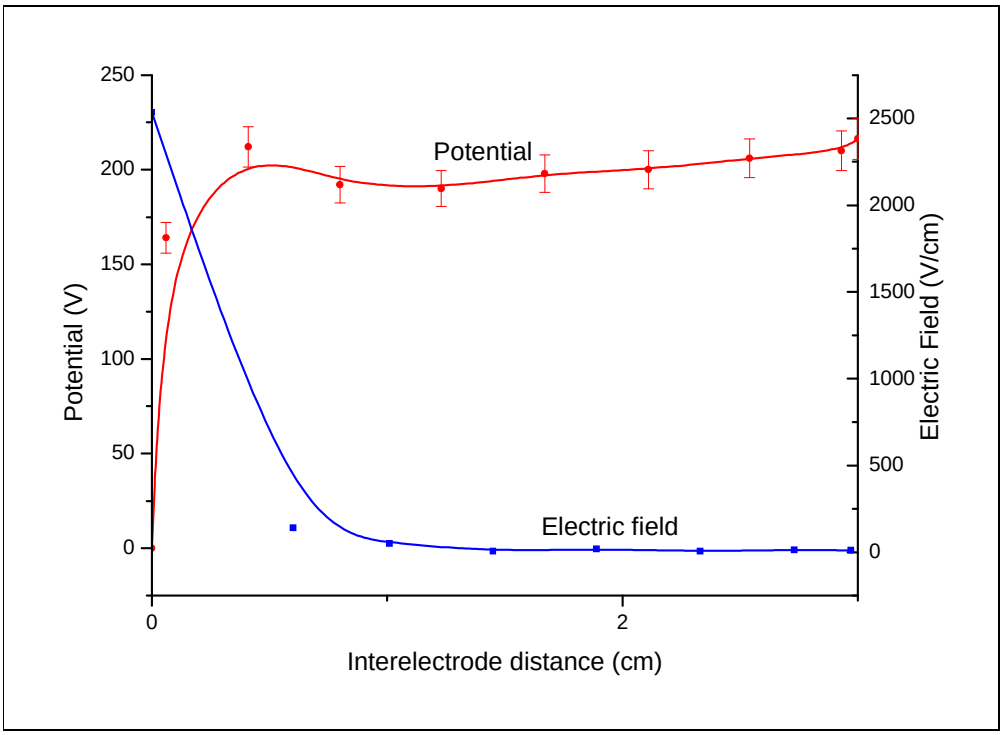

Figure 4.3: Experimentally measured potential distribution together with the electric field distribution for the same discharge as in Figure 4.2.

The DC glow discharge as described above has been simulated using XPDP1 in the voltage driven mode. In order to obtain the experimentally observed discharge current range of 5 to 30 mA, the current limiting resistance R_L was adjusted accordingly. As the material of the electrode used was copper, by referring to Brown [24], the constant effective ion-induced secondary electron emission coefficient (SEEC) is much less than one for glow discharge with copper as electrode material. Since it is the emission of secondary electrons from the cathode by ion impact which keeps the plasma sustainable, the value of SEEC is expected to have a large influence on the steady state of the discharge. However, the exact value depends on the electrode material and also the "dirtiness" of the metallic electrode [6].

In our case, we have tested two values of the SEEC, namely 0.2 and 0.09. 0.09 is near to the most commonly quoted value which is near to 0.01, and 0.2 is for comparison. The simulated *I-V* characteristics obtained by taking SEEC = 0.2 at various discharge conditions have been plotted together with the experimental results as shown in Figure 4.4.

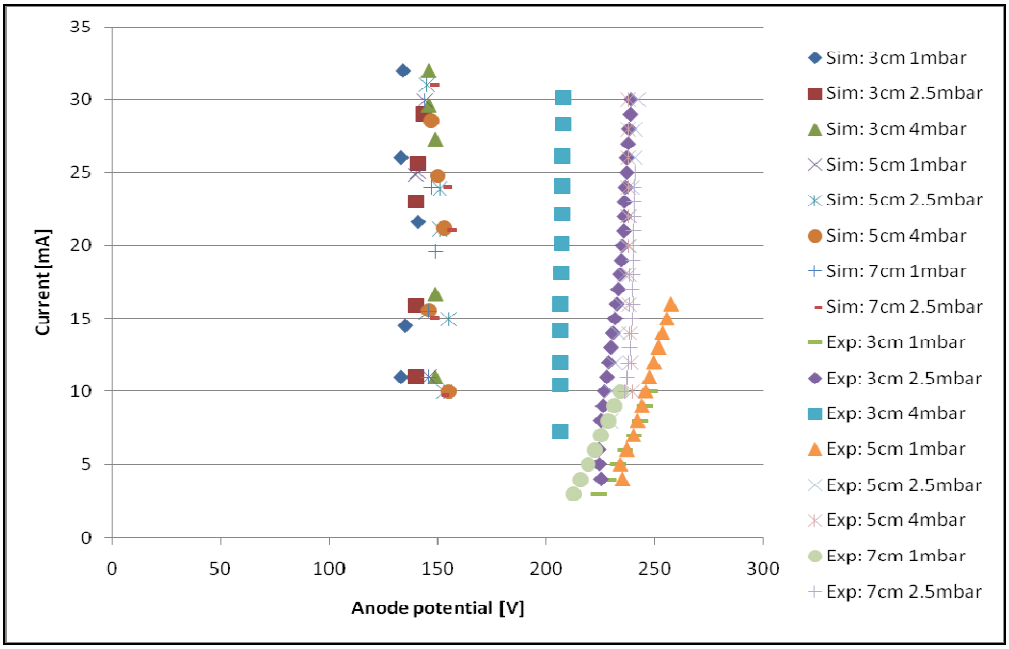

Figure 4.4: Comparison of experimental and simulated *I-V* characteristics of DC glow discharge. (simulation with SEEC = 0.2, V = 366 V)

While the simulated results indicated the existence of normal glow discharge for the range of condition similar to the experiments, the simulation predicted a lower anode potential of around 150 V for all the conditions investigated experimentally, including the conditions when the operating pressure is set at 1 mbar. The anode potential can be raised to near 200 V but using a lower value of SEEC. Figure 4.5 shows the simulated *I-V* characteristics obtained by setting SEEC = 0.09 while the power supply voltage is set at 450 V in order to achieve the same range of discharge current of 10 to 30 mA. It is clear that the case of SEEC = 0.09 is able to give a

better agreement with the experimental data. Figure 4.6 and 4.7 are the trend of the potential and electric field distribution across the electrodes respectively.

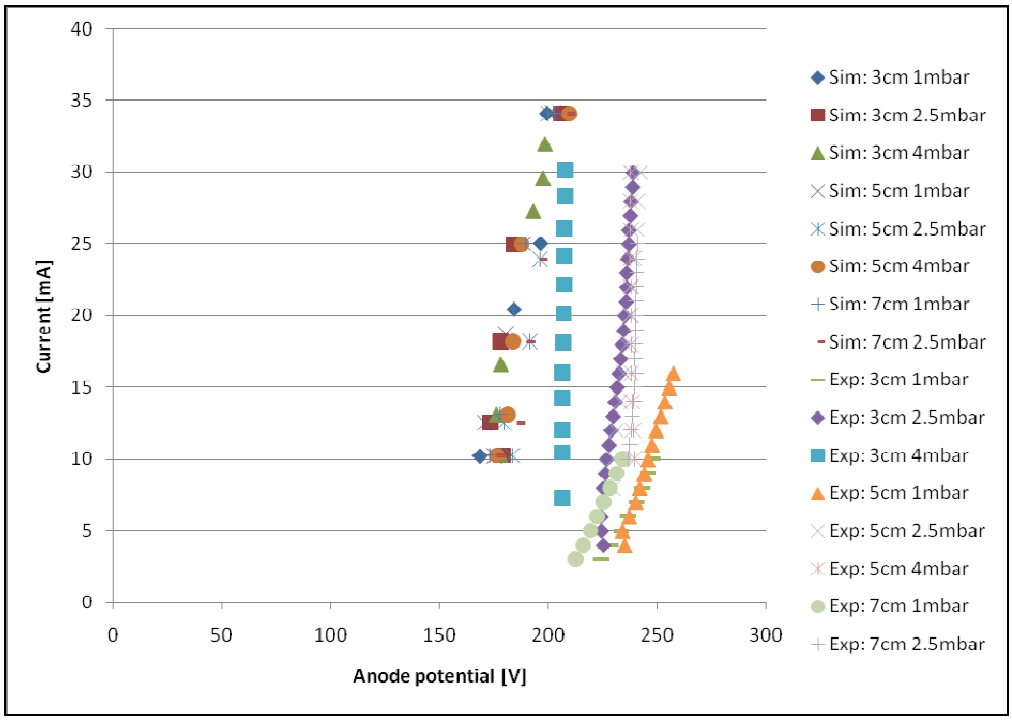

Figure 4.5: Comparison of experimental and simulated I-V characteristics of DC glow discharge. (simulation with γ = 0.09, V = 450 V)

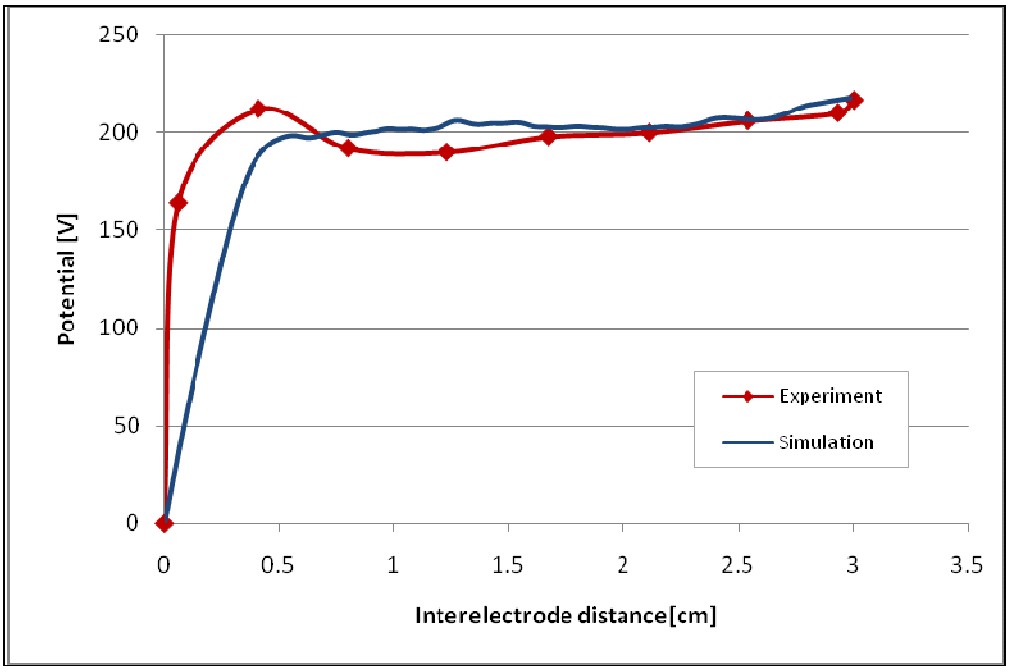

Figure 4.6: Comparison of experimental and simulated potential distribution across the electrodes for normal glow discharge (SEEC = 0.09, *V* = 450 V).

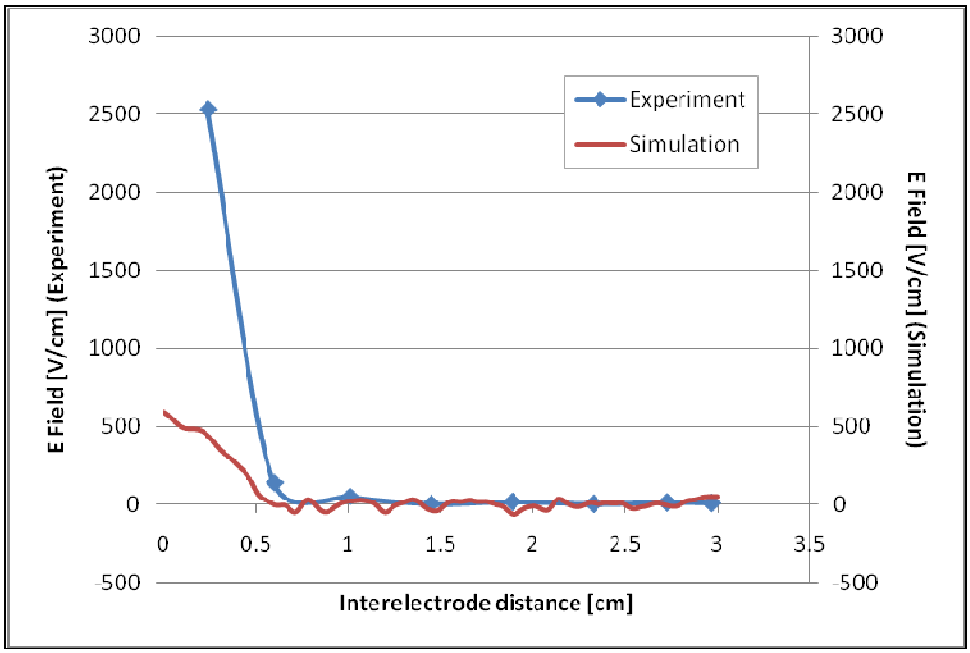

Figure 4.7: Comparison of experimental and simulated electric field distribution across the electrodes for normal glow discharge (SEEC = 0.09, *V* = 450 V).

4.1.2 Electron temperature, electron density and electron energy distribution function

In the experiments carried out by Safaai [3], the electron temperature and electron density of the argon glow discharge plasma were measured by using a single Langmuir probe. Figures 4.8 and 4.9 show how these plasma parameters, both measured experimentally, vary with the discharge current. In the Langmuir probe technique, the electron temperature of the plasma is determined from the electron retardation region of the *I-V* characteristic curve with the assumption that the plasma is Maxwellian. The electron density is determined from the electron saturation current when the probe potential is equal to the plasma potential. From the XPDP1 simulation, the electron temperature (in eV) was taken to be the average kinetic energy of the electrons in the bulk of the plasma. The simulated "electron

temperature" is plotted together with the experimentally measured electron temperature in Figure 4.8. We feel that the agreement between the experiment and simulation is acceptable, since the experimental values are obtained at a localized point in the plasma, while the simulation gives the average over the bulk of the plasma. On the other hand, the comparison between the experimental and simulated values of the electron density shows different trends in the variation of the electron density with discharge current. While the experimental electron density is constant over the range of discharge current, the simulated electron density is observed to drop when the discharge current increases. This is due to the large variation of the simulated electron density within the plasma column as can be seen from Figure 4.10. The electron density measured experimentally is the average value at the location of the probe. The non-homogeneity could be incorporated into the simulation by introducing non-uniform grid.

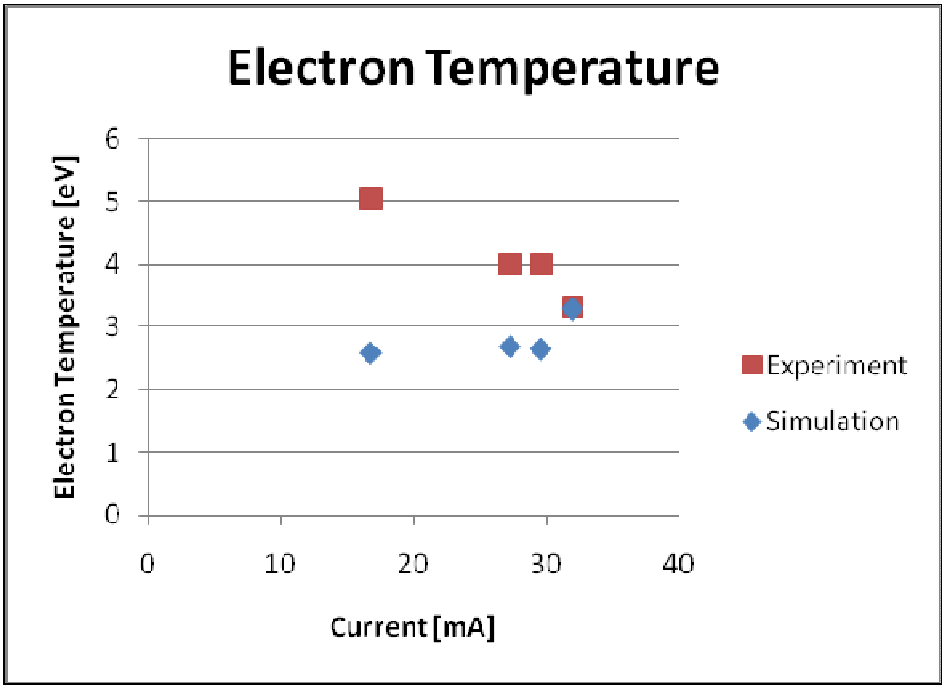

Figure 4.8: Electron temperature of argon plasma for discharge currents of 16.67, 27.3, 29.6, 32 mA and at pressure of 4 mbar Ar gas filling.

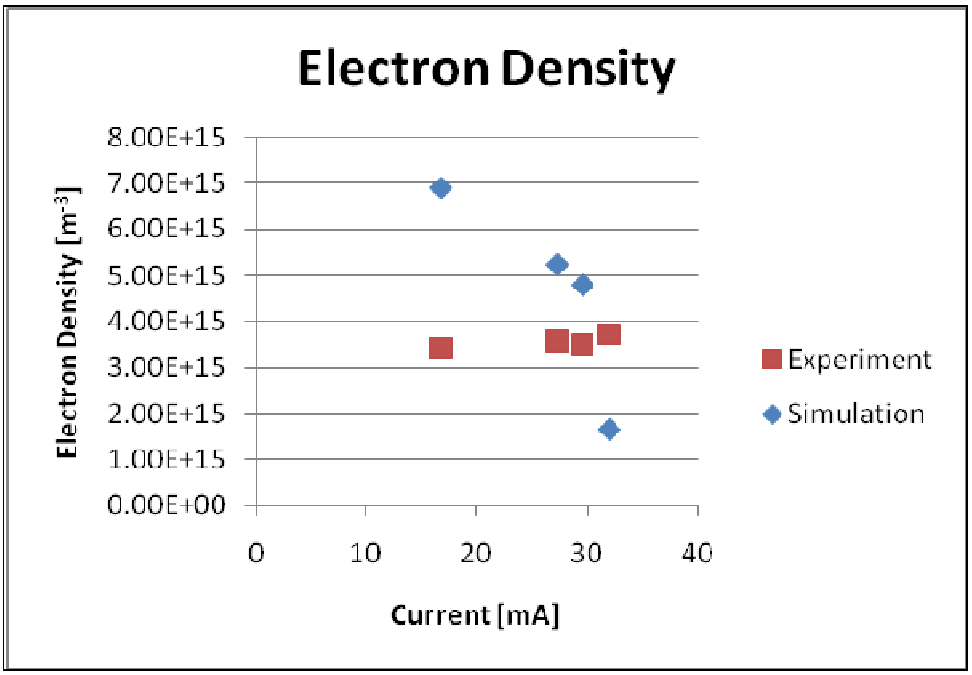

Figure 4.9: Electron density of the argon plasma for discharge current of 16.67, 27.3, 29.6, 32 mA and at pressure of 4 mbar Ar gas filling.

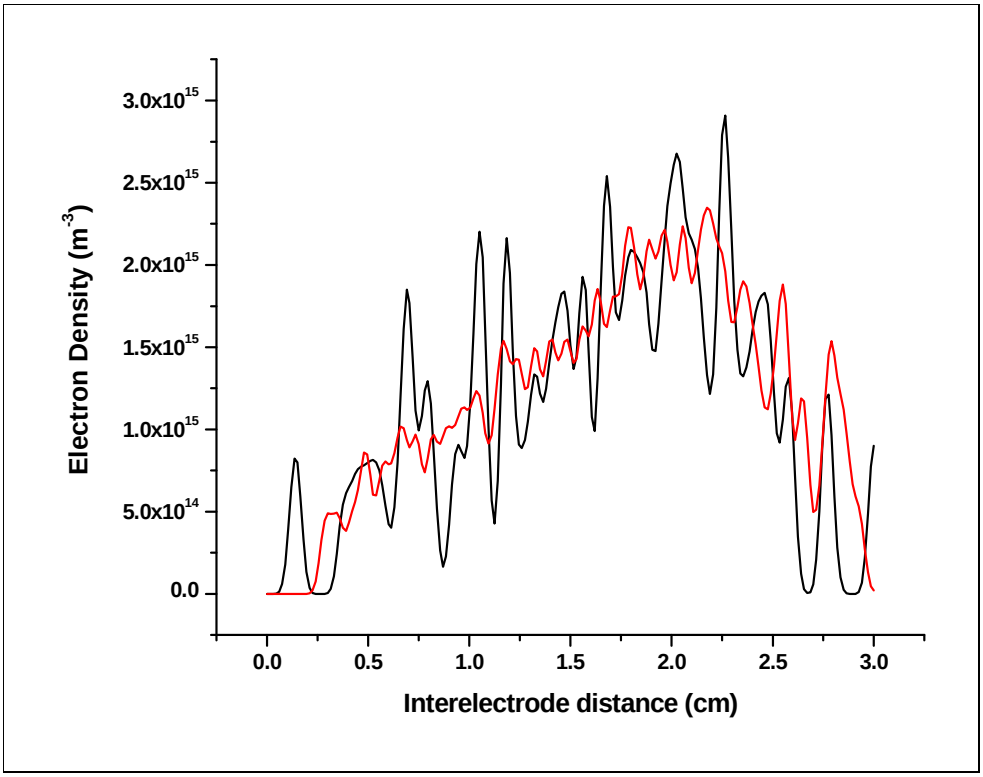

Figure 4.10: Simulation results of plasma density profiles for discharge current of 32 mA at pressure of 4 mbar. Black line: electron density. Red line: ion density.

The electron energy distribution functions obtained from the simulation (SEEC = 0.09, V = 450 V) are shown in Figures 4.11 and 4.12. Figure 4.12 is plotted in the semilogarithmic scale. If the electron energy distribution is Maxwellian, the semilog plot should give a linear curve on the right hand side of the peak [25]. Figure 4.13 shows an ideal Maxwellian distribution in semilog scale and its comparison with the simulation result for a discharge with discharge current of 32 mA. It shows that the simulated electron energy distribution is not Maxwellian.

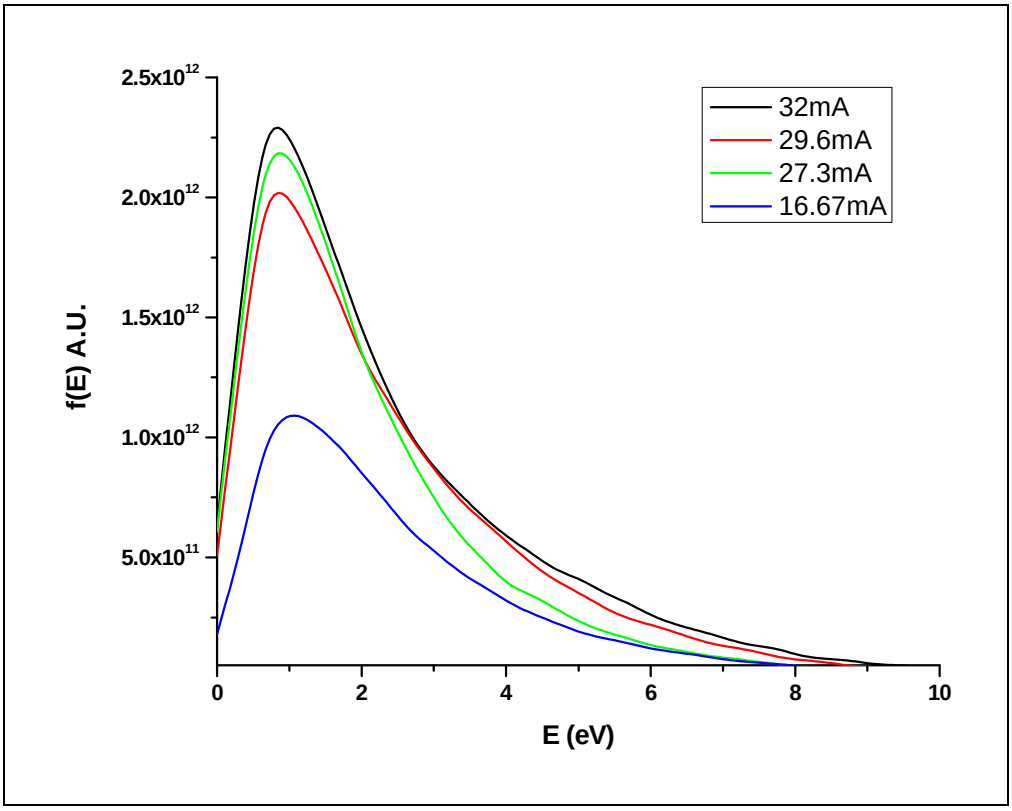

Figure 4.11: Simulated electron energy distribution functions for discharges with current of 16.67 mA to 32 mA, plotted in linear scale.

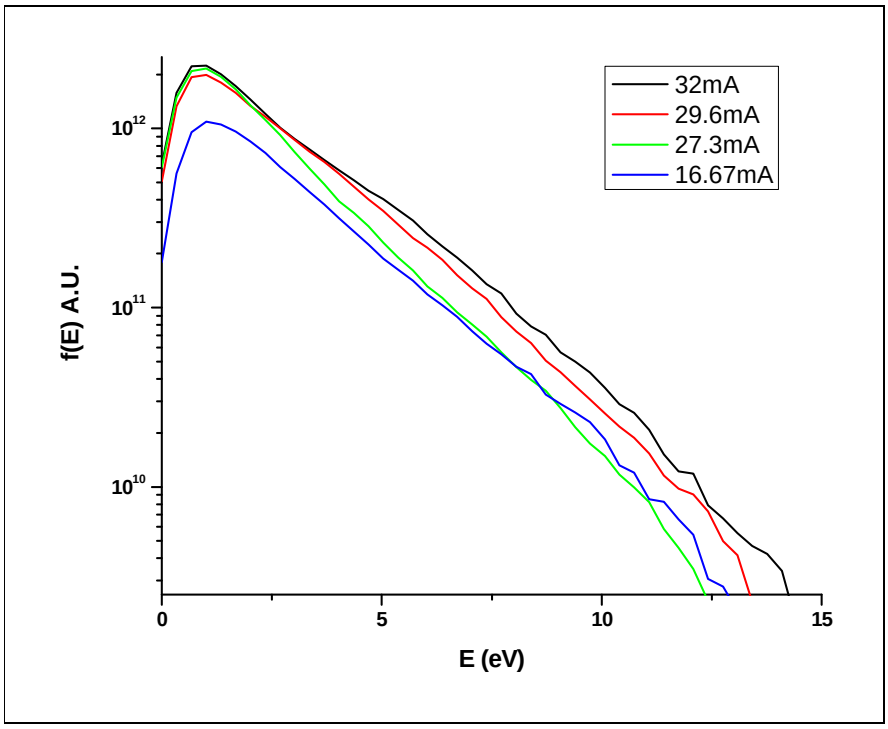

Figure 4.12: Simulated electron energy distribution functions for discharges with current of 16.67 mA to 32 mA, plotted in semilogarithmic scale.

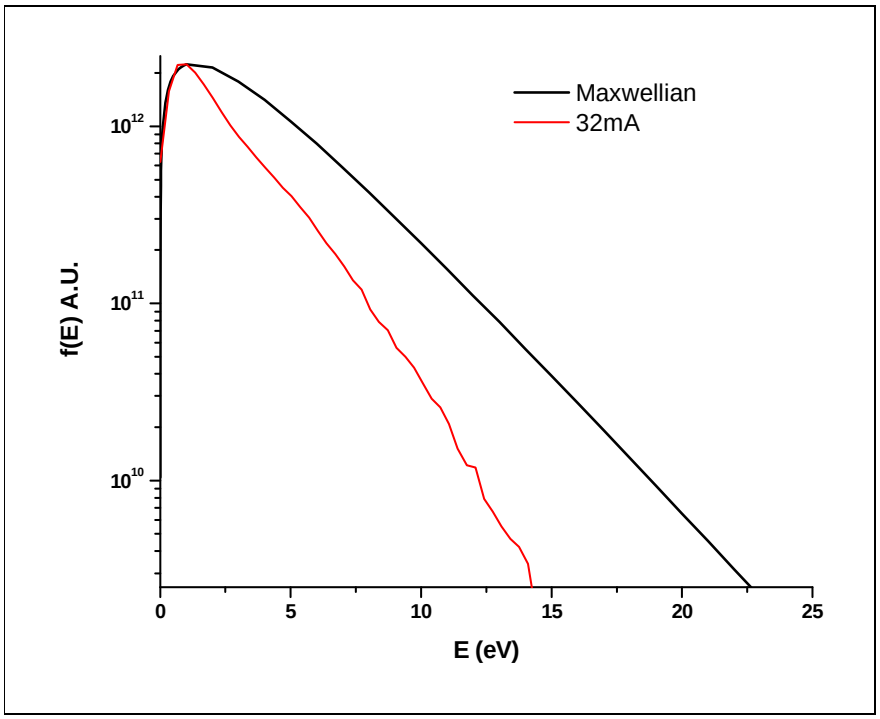

Figure 4.13: An ideal Maxwellian distribution function plotted in semilog scale (for T_e = 3.07 eV), compared to the simulation result for discharge with current of 32mA.

An attempt has been made to compare the simulated electron energy distribution functions with those measured experimentally. For this purpose, the values of the experimental electron energy distribution function, which are expressed as arbitrary unit, have been normalized to those obtained from the simulation. Figure 4.14 shows such comparison for discharge with current of 32 mA, which illustrates good agreement between the two.

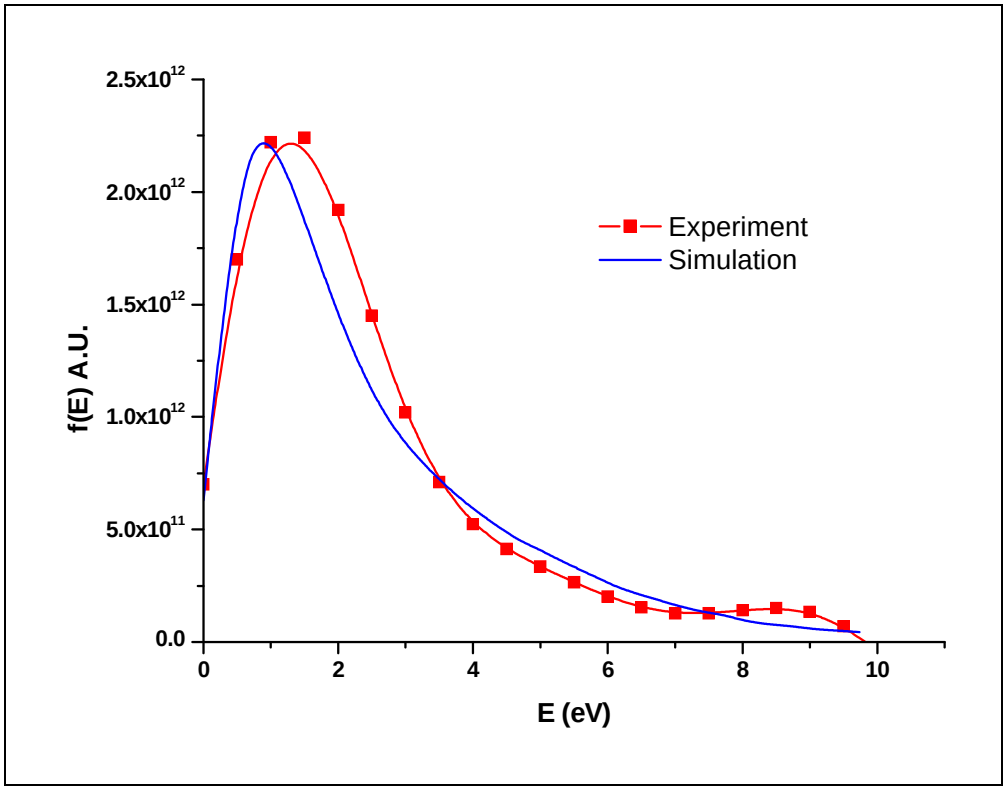

Figure 4.14: Electron energy distribution for pressure 4 mbar, inter-electrode gap of 3 cm and discharge current of 32 mA from the experimental results [3] compared with simulation (SEEC = 0.09, V = 450 V).

4.1.3 Fundamental plasma processes

As discussed in Chapter 3, the XPDP1 takes into consideration of various fundamental plasma processes in its simulation of the gas discharge. These include both electron-neutral and ion-neutral collisions. In a glow discharge, for electron-neutral collisions, the important processes are scattering, excitation and ionization; while for ion-neutral collisions, charge exchange and scattering are dominant. The probabilities of occurrence (cross-section) for these processes as a function of interelectrode position are generated from the simulation and are shown in Figures 4.15 to 4.17 below. The simulation was done with SEEC = 0.2, discharge voltage *V* = 366 V while the discharge current was varied from 16.67 mA to 32 mA. The interelectrode separation was set at 3 cm.

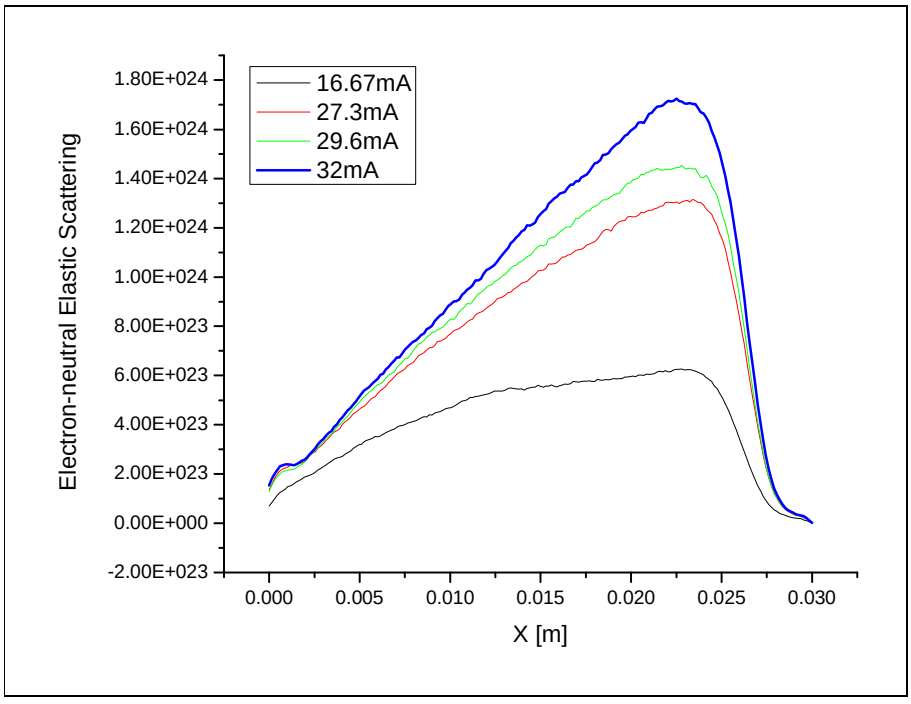

Figure 4.15: Electron-neutral collision: Elastic Scattering. (Cathode at X = 3 cm)

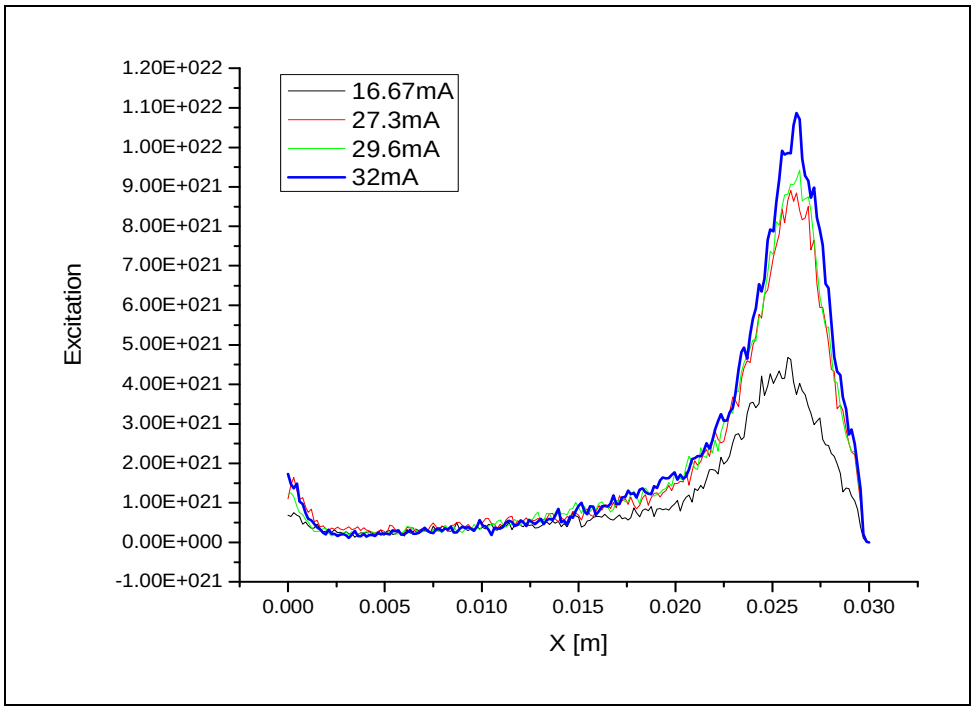

Figure 4.16: Electron-neutral collision: Excitation. (Cathode at X = 3 cm)

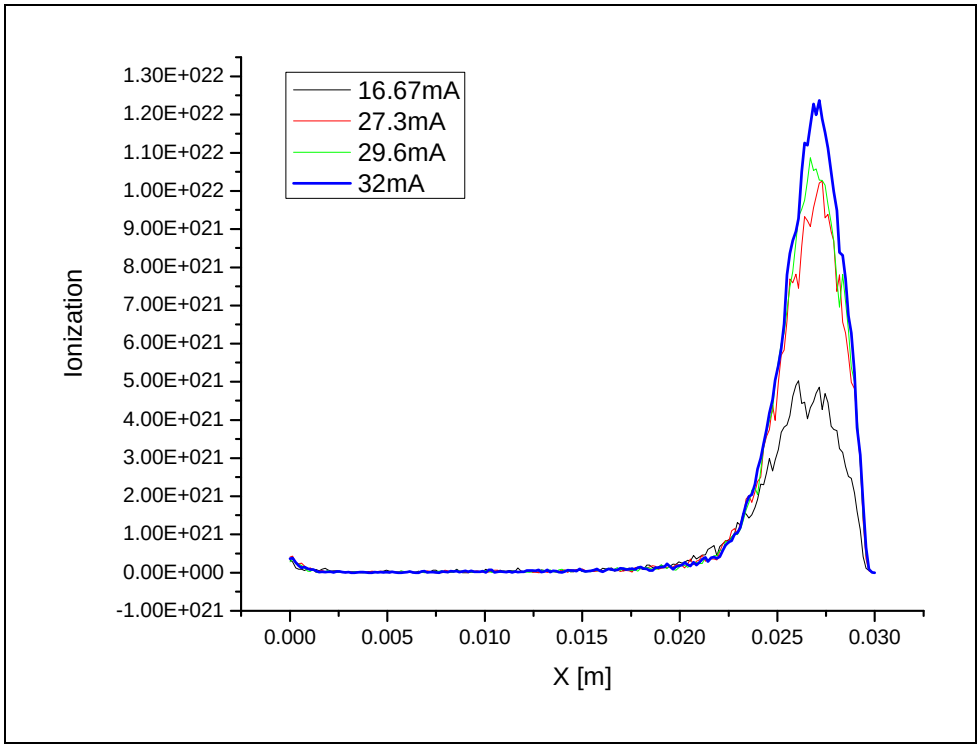

Figure 4.17: Electron-neutral collision: Ionization. (Cathode at X = 3 cm)

In Figure 4.15, it is shown that the elastic scattering, which is due to elastic collision between electron and neutral, has the maximum probability at the Faraday dark space region of the glow discharge, where the electron energy is low. The electron loses its energy and slow down after passing through the negative glow region. Hence in the Faraday dark space region, besides recombination and diffusion to the wall, the electron-neutral elastic scattering rate is the highest. On the other hand, excitation and ionization have large cross-sections in the negative glow within the cathode fall region as can be seen from Figures 4.16 and 4.17. For higher discharge current, the rate of occurrence of all these processes are observed to increase as expected.

The collision between ion and neutral in the glow discharge is capable of producing charge exchange and scattering processes only due to their low kinetic energy. The highest occurrence is in the Crookes dark space which is within the cathode fall region (plasma sheath). The rates of occurrence as a function of axial position are as shown in Figures 4.18 and 4.19.

The rate of energy deposition in the glow discharge is calculated from the product of current density and electric field at each location in the glow discharge. This is shown in Figure 4.20. The highest rate of energy deposition by the electrons is within the plasma sheath as expected. There are two principal heating mechanisms in plasma discharge: ohmic heating in the plasma bulk and stochastic heating in the sheath. The power deposition profiles in Figure 4.20 show that the major mechanism for electrons heating is stochastic heating, as the power deposition mainly in the sheath region. Besides, the power deposition rises when discharge current rises.

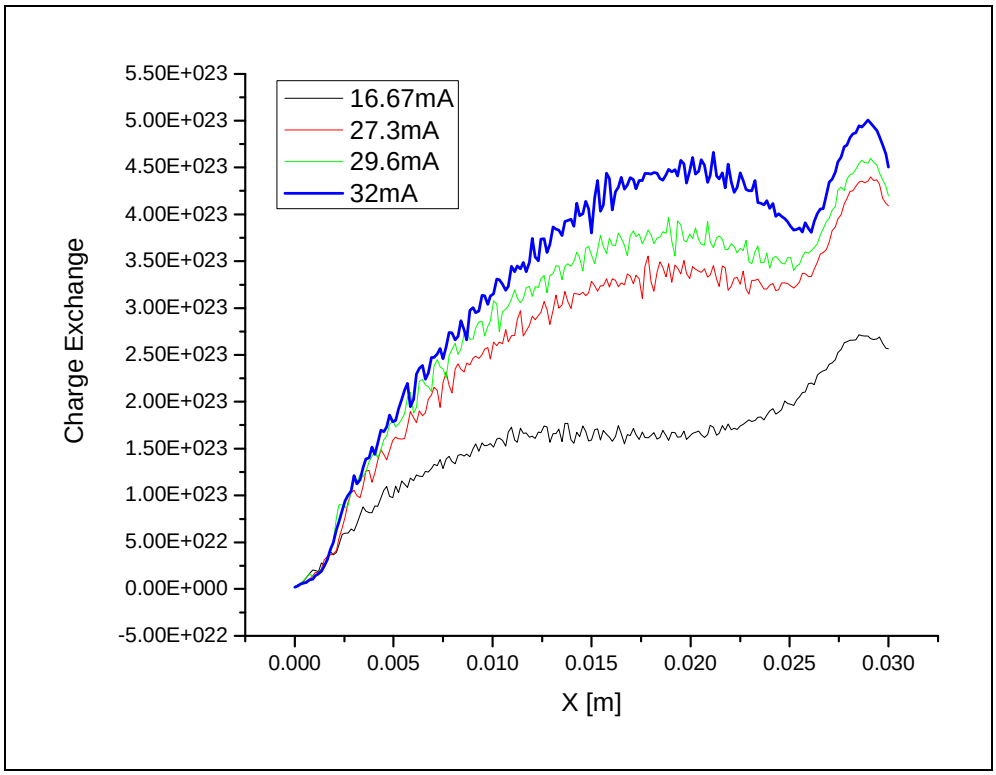

Figure 4.18: Ion-neutral collision: Charge Exchange (Cathode at X = 3 cm)

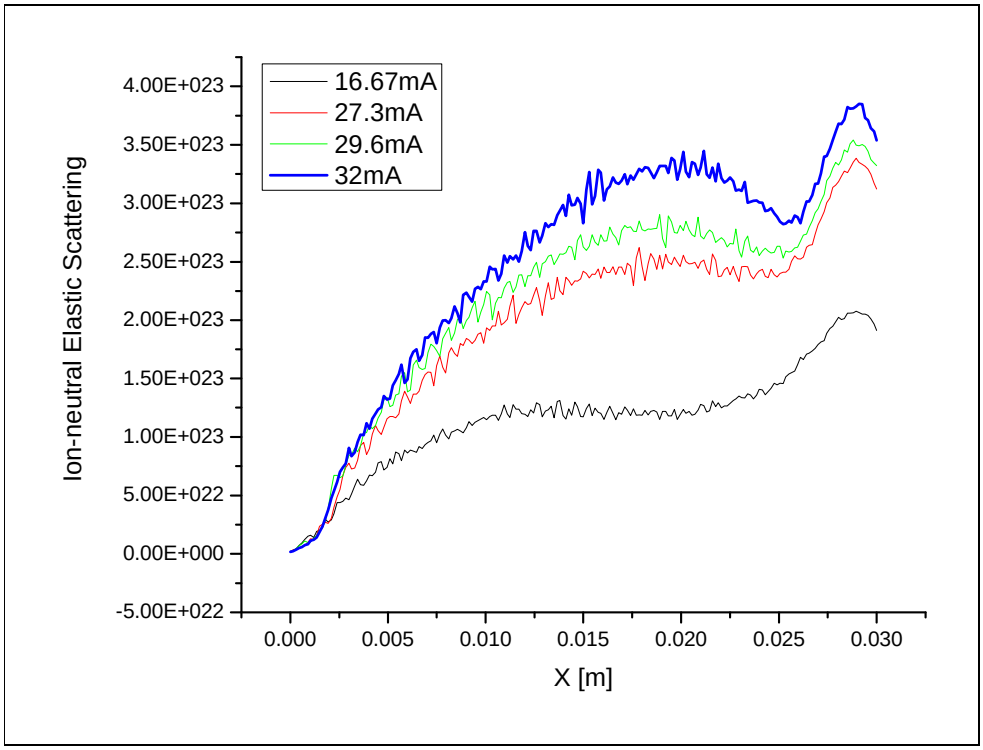

Figure 4.19: Ion-neutral collision: Elastic Scattering (Cathode at X = 3 cm)

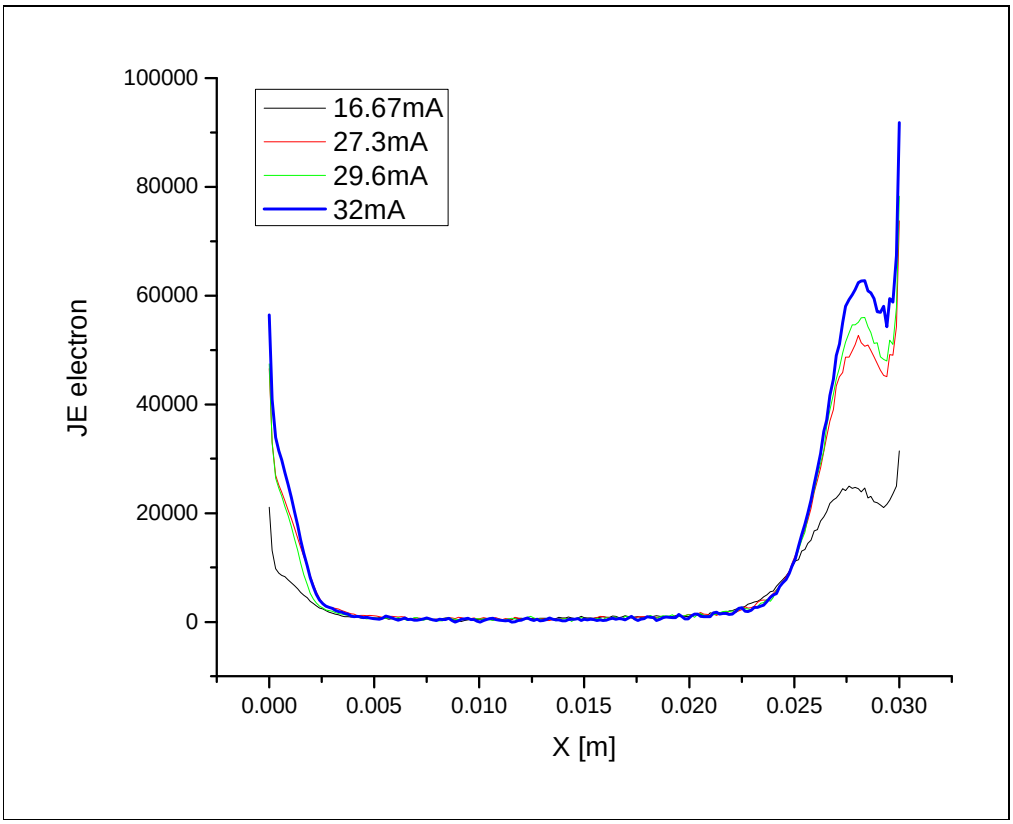

Figure 4.20: Power deposition for electron (Cathode at X = 3 cm)

4.5 Effects of various experimental parameters on discharge characteristics

Exploiting the convenience provided by the ease of changing the experimental parameters in the XPDP1 simulation, we can attempt to investigate the possible effects of various experimental parameters on the characteristics of the glow discharge. The following experimental parameters are investigated here to illustrate the flexibility of the code.

4.5.1 Effect of Interelectrode gap length

The simulation was performed with SEEC = 0.2, V = 366 V, I = 32 mA. Figure 4.21 shows the potential and electric field distribution across the interelectrode spacing.

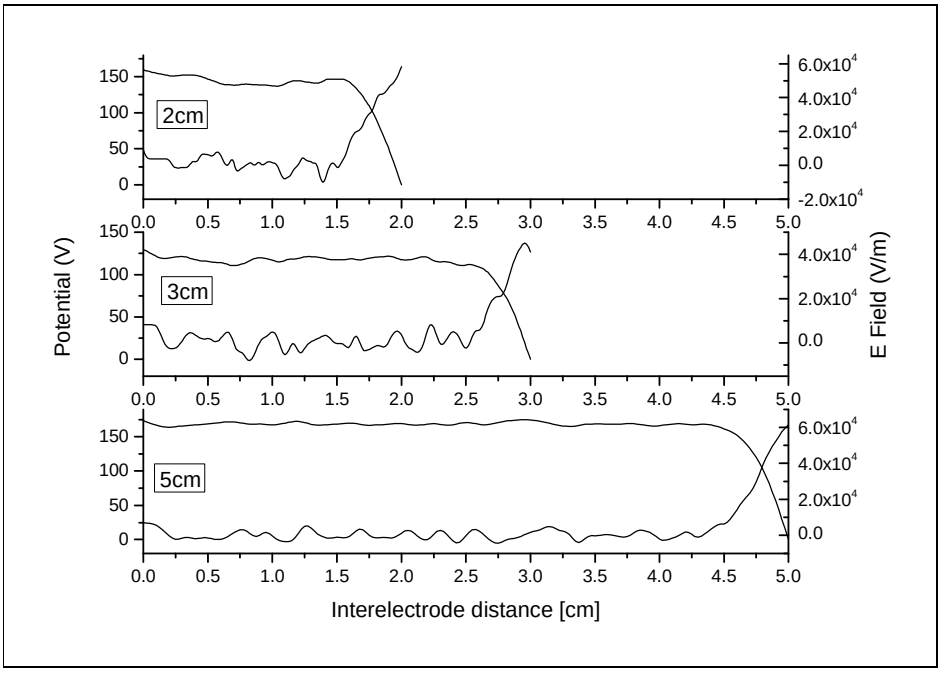

Figure 4.21: Potential and electric field profiles for discharges obtained with interelectrode distance of 2 cm to 5 cm (pressure 3 Torr).

As can be observed from Figure 4.21, the cathode fall region (plasma sheath) thickness remains the same, while the length of the positive column varies with the change of interelectrode gap length. The electron density of the plasma in the bulk of the plasma increases slightly when the interelectrode gap length increases, while the electron temperature is decreased. Table 4.1 gives a summary of the results obtained from the simulation.

Table 4.1: Simulation results showing the effect of interelectrode gap length on the characteristics of the DC glow discharge.

Interelectrode gap length [cm]	Current [mA]	Potential (Glow voltage) [V]	Power [W]	Electron Temperature [eV]	Electron density [m^{-3}]
2	31.90	143	4.12	3.38	1.39E15
3	31.90	146	4.16	3.07	1.74E15
5	31.60	149	4.18	2.81	2.02E15

The electron energy distribution functions are of the Druyvesteyn type for all the three cases of interelectrode gap length, as illustrated in Figure 4.22.

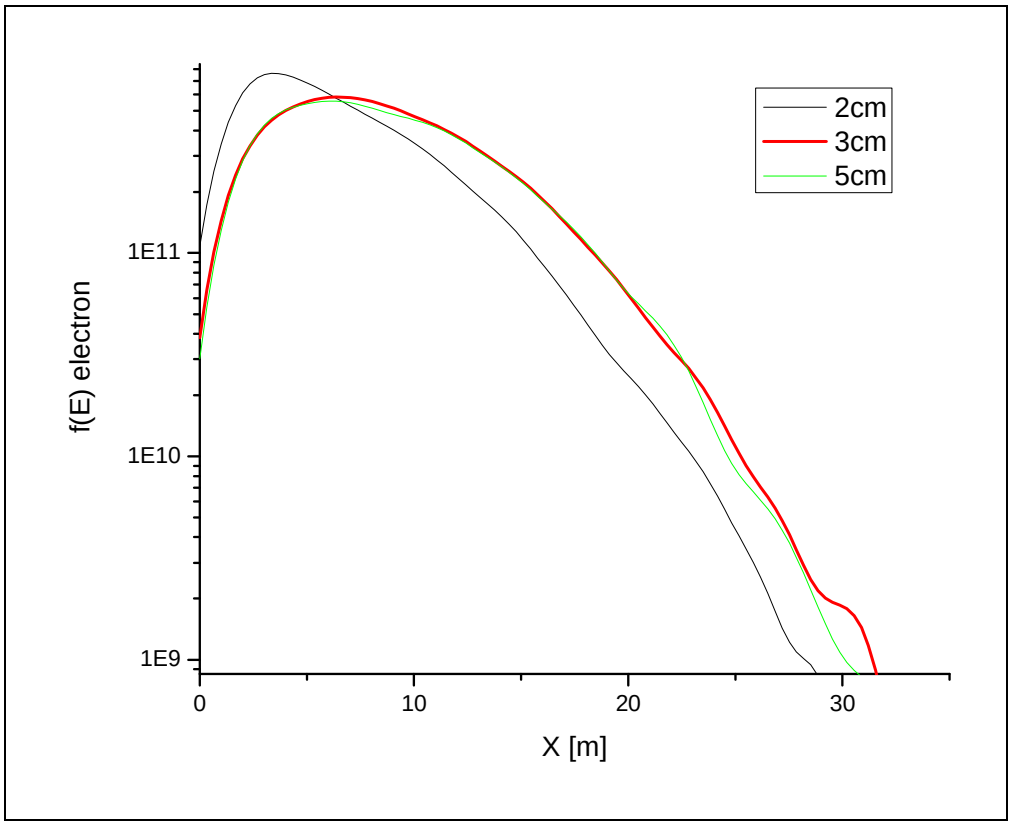

Figure 4.22: Electron energy distribution function for discharge with interelectrode gap length of 2 cm, 3 cm and 5 cm.

4.5.2 Effect of operating pressure

Similarly, the effect of operating pressure on the characteristics of the DC glow discharge has been investigated. Table 4.2 shows the summary of the results obtained. The operating pressure was varied within the range of 0.5 Torr to 10 Torr. The glow voltage is lower for pressure of 0.5 Torr. The electron temperature of the plasma for pressure of 0.5 Torr is also lower. However, the electron energy distribution for discharge with 0.5 Torr operating pressure seems to be more Maxwellian as compared to the three higher pressure cases as shown in Figure 4.23.

Table 4.2: Simulation results showing the effect of operating pressure on the characteristics of the DC glow discharge.

Discharge pressure [mbar]	Current [mA]	Potential (Glow voltage) [V]	Power [W]	Electron Temperature [eV]	Electron density [m^{-3}]
0.5	34.10	130.41	4.06	2.82	2.36E15
3	31.90	146.12	4.16	3.07	1.75E15
5	31.90	151.41	4.20	3.06	1.65E15
10	31.90	151.41	4.16	3.06	1.72E15

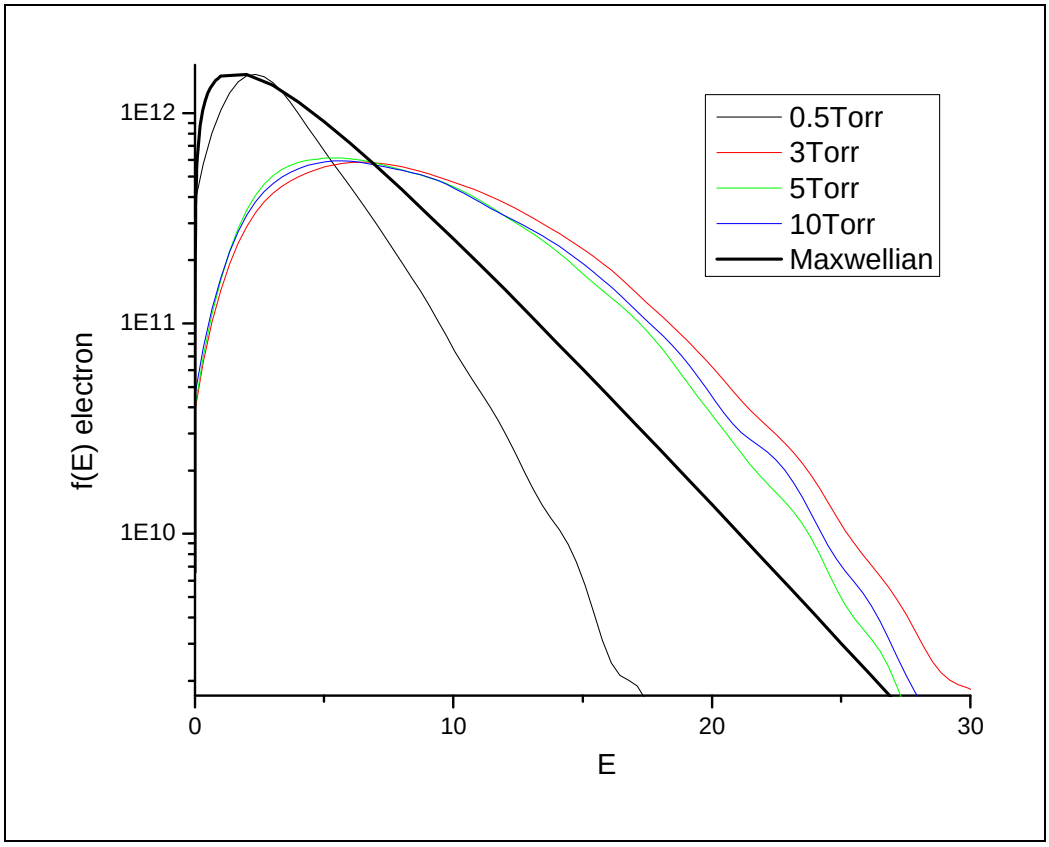

Figure 4.23: Electron energy distribution profiles of discharge pressure 0.5~10Torr (interelectrode gap length 3 cm).

4.5.3 Effect of operating voltage

Variation of the operating voltage gives rise to an increase in the discharge current while maintaining the operating pressure at 4 mbar argon and interelectrode distance of 3 cm. The distribution of potential and electric field for operating voltage of 300 V, 366 V and 500 V and all with SEEC = 0.2 are shown in Figure 4.24, while Table 4.3 gives the summary of various parameters obtained from the simulation results.

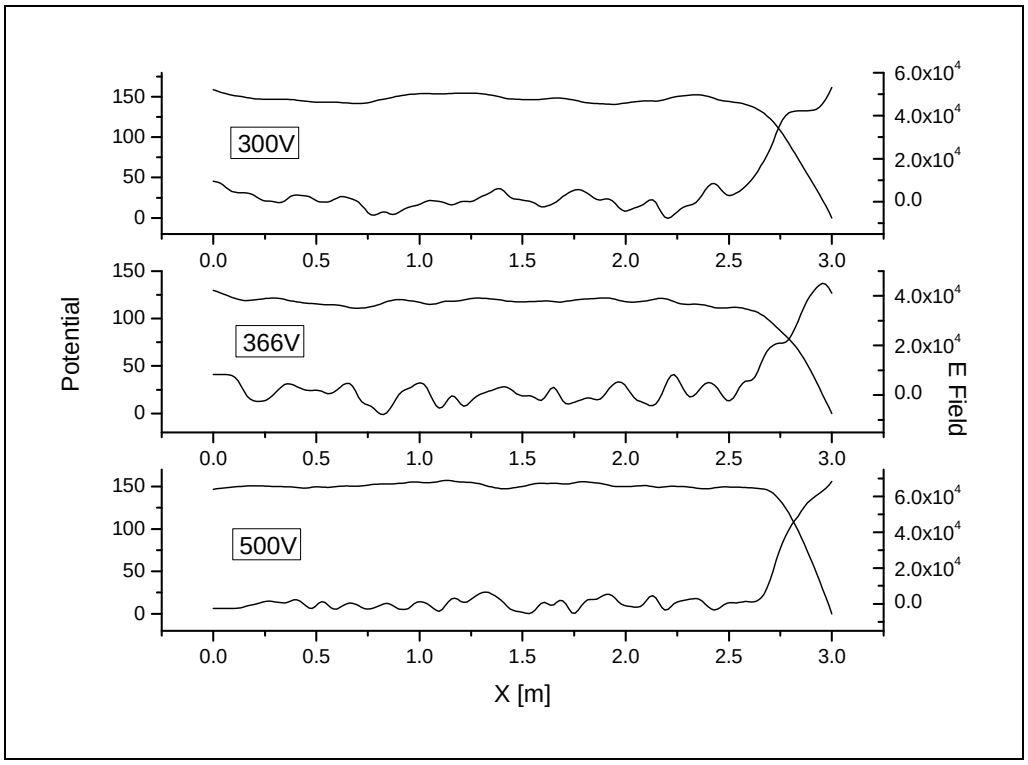

Figure 4.24: Potential and electric field profiles of driving voltage 300V~500V.

Table 4.3: Simulation results showing the effect of operating voltage on the characteristics of the DC glow discharge

Driving voltage [V]	Current [mA]	Potential (Glow voltage) [V]	Power [W]	Electron Temperature [eV]	Electron density [m^{-3}]
300	20.8	152.87	2.87	2.89	7.67E14
366	31.9	146.12	4.16	3.07	1.74E15
500	49.7	143.66	6.87	3.18	3.79E15

As shown in Figure 4.24, the sheath thickness seems to decrease slightly in the case of 500 V discharge as compared to 300 V and 366 V. This indicates that when the driving voltage increases, the sheath thickness decreases. When the driving voltage increased from 300 V to 500 V, the electron density increased as well as the resulting current supply (Table 4.3). Besides, in Table 4.3, the electron temperature is observed to be increased when the driving voltage increases.

The electron energy distribution functions obtained for simulation using the three operating voltages are shown in Figure 4.25, and all of them are found to be of the Druyvesteyn type. The peak of the curve of all voltages has an increase in magnitude when the voltage increases.

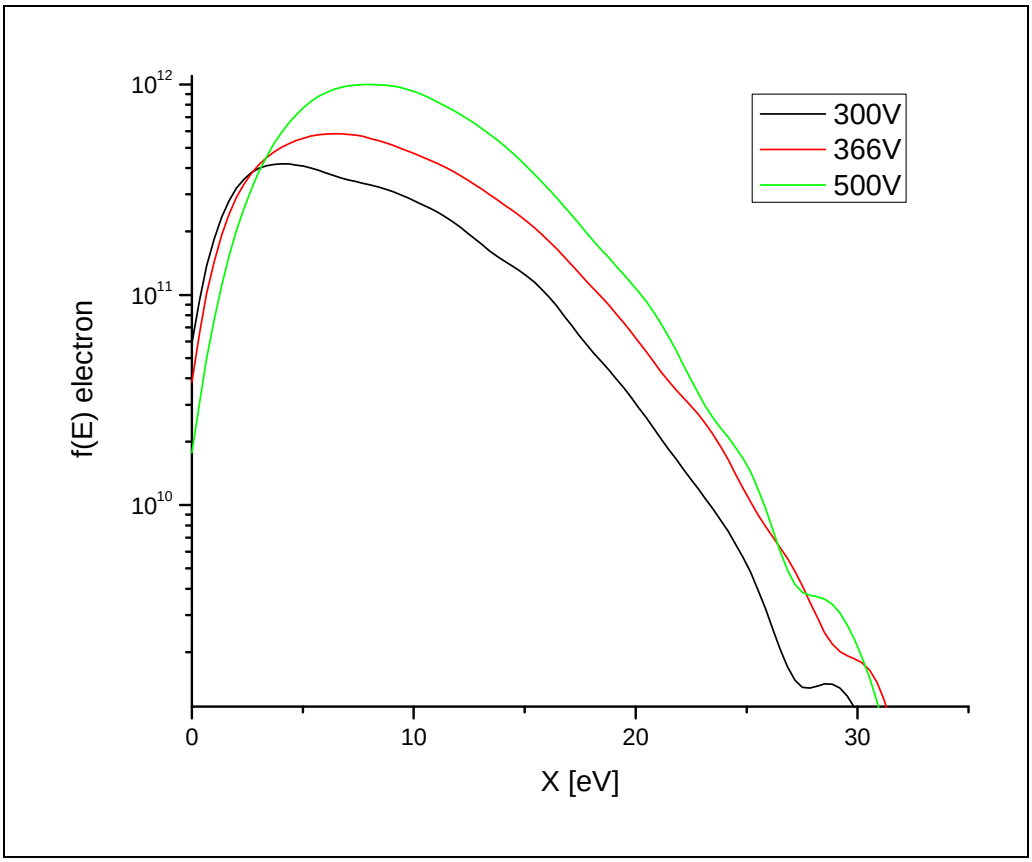

Figure 4.25: Electron energy distribution functions obtained from simulation using driving voltage of 300 V, 366 V and 500 V.

4.6 Simulation of RF Glow Discharge - comparison of DC glow discharge with RF glow discharge

The application of the XPDP1 simulation code had been extended to study discharges powered by radio-frequency (RF) voltage source and comparison of the results obtained with that of the DC glow discharge discussed earlier was made. The simulation of the RF glow discharge was done by changing the DC voltage to AC voltage, and putting a non-zero magnitude of frequency. The parameters used in the simulation were chosen to match that for the 32 mA DC glow discharge. The interelectrode distance was 3 cm, pressure 4 mbar, filling was argon gas, peak supplied voltage of 366 V voltage and 7.65 kΩ as the external circuit resistance.

The various plasma properties obtained from the simulation are summarized in Table 4.4 side by side with those obtained for DC glow discharge. It can be seen that glow discharge with similar plasma condition can be obtained by using both DC power source and RF power source.

Table 4.4: Various parameters for DC and RF glow discharge obtained from the simulation.

Discharge mode	Current [mA]	Potential (Glow voltage) [V]	Power [W]	Electron Temperature [eV]	Electron density [m^{-3}]
DC	31.9	146	4.16	3.07	1.74E15
RF	39.5	109	2.00	3.50	1.45E15

One significant difference between the DC glow discharge and the RF glow discharge is that since the power source is time-varying in the case of RF glow discharge, the potential at one of the electrodes is changing sinusoidally between positive maximum and negative maximum at a fixed frequency of 13.56 MHz, while the other electrode is fixed at ground potential. Hence the discharge current is also changing with time in a sinusoidal manner. As the transit time of the electrons between the electrodes is longer than the electric field reversal time the electrons will be made to spend longer time in the inter-electrode space before reaching the other electrode.

Figure 4.26 illustrate the potential distribution within the inter-electrode space of a RF glow discharge at (a) positive voltage, (b) zero voltage, and (c) negative voltage. Cases (a) and (c) are identical to those of a DC glow discharge where the voltage applied to the left hand electrode (at x = 0) is at either maximum positive voltage or maximum negative voltage respectively, while the potential at x = 3 cm is maintained at ground potential. However, for the case when the voltage applied is passing through zero giving rise to the situation where both electrodes are at zero potential, the potential distribution is as shown in Figure 4.26 (b).

Corresponding, the distribution of the electric field in the inter-electrode region for the three cases are shown in Figure 4.26.

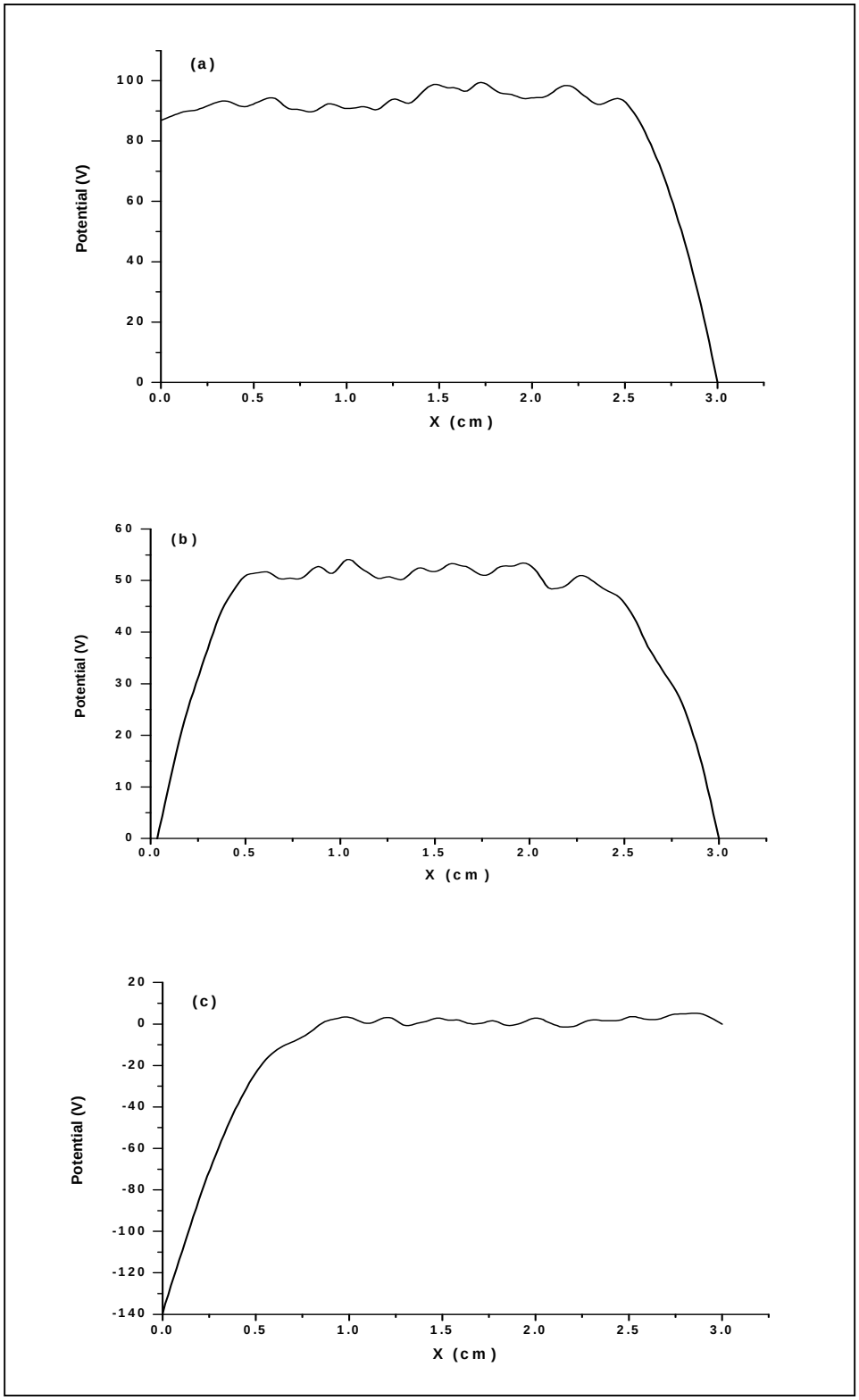

Figure 4.26: Potential distribution across the electrodes when the supply voltage at the left hand electrode is at (a) positive maximum, (b) zero, and (c) negative maximum.

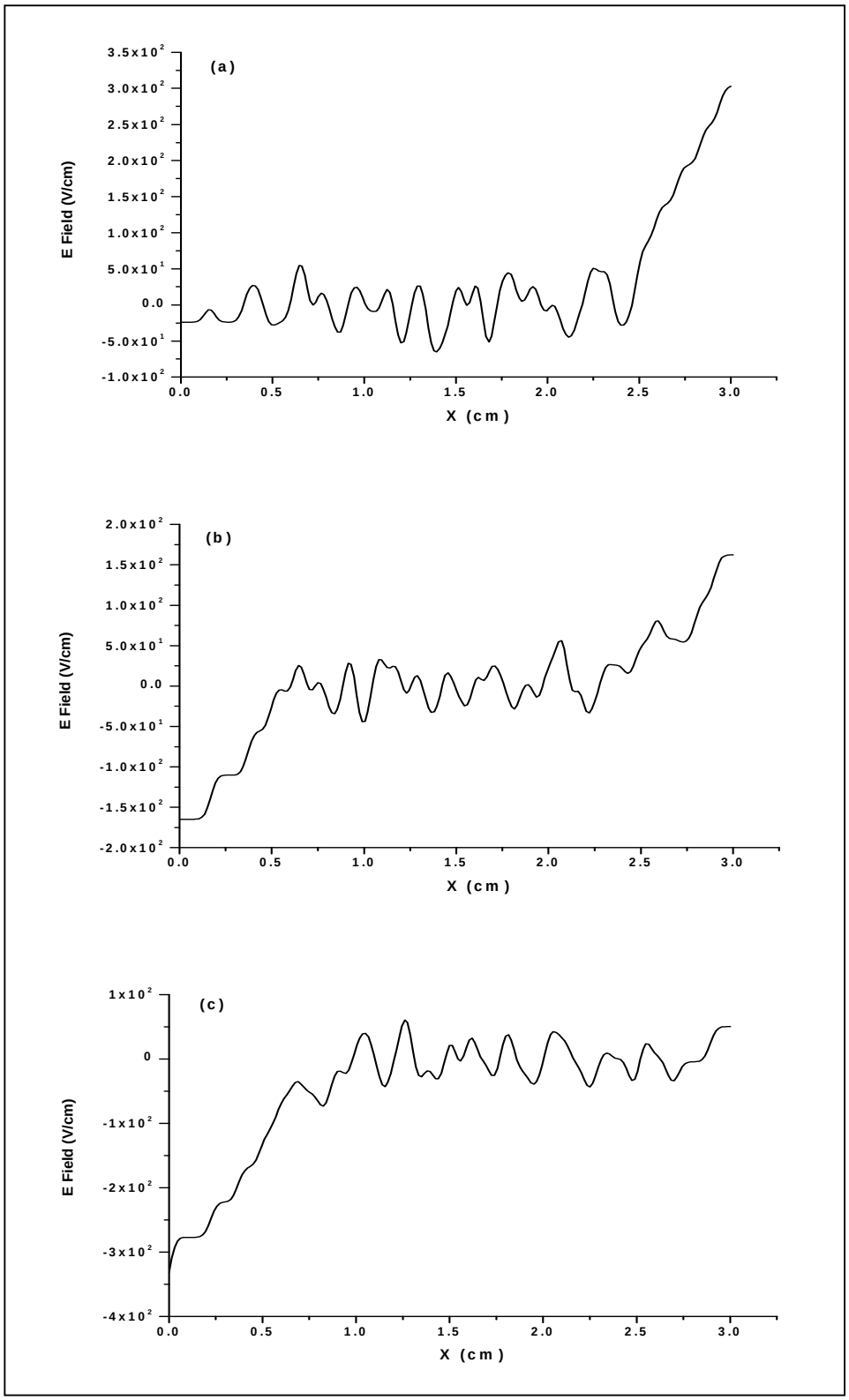

Figure 4.27: Inter-electrode electric field distribution for the three cases corresponding to those in Figure 4.26.

Figure 4.28 shows the electron energy distribution of the DC and RF glow discharges for comparison. Note that the graph for RF discharge was obtained at the time when the discharge current passed through zero. It is commonly known that for an alternating current discharge at RF frequency, the plasma is alive even when the current is passing through zero, as can be seen from the fact that the plasma potential is non zero at the instant when the current passes through zero (Figure 4.26(b)). In fact, the electron energy distribution functions as shown in Figure 4.28 remains almost the same although the discharge current is alternating as long as the discharge has reached steady state. The same is also observed for the distribution of cross section of other fundamental processes such as scattering, excitation and ionization. These are illustrated in Figure 4.29, Figure 4.30 and Figure 4.31.

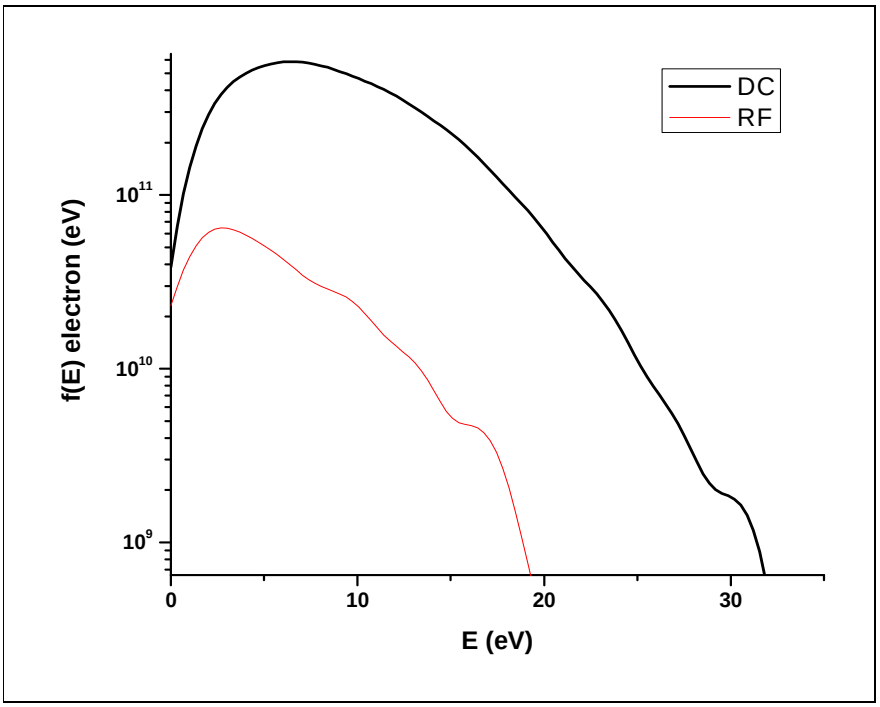

Figure 4.28: Comparison of electron energy distribution functions of DC and RF discharges.

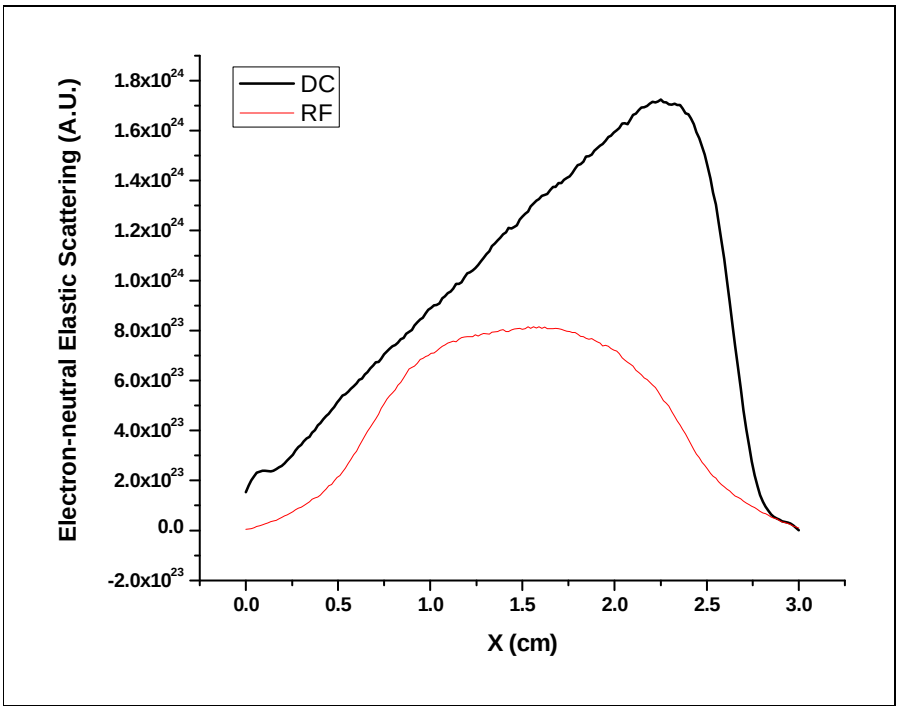

Figure 4.29: Comparison of elastic scattering cross sections for electron-neutral collision in DC and RF discharges.

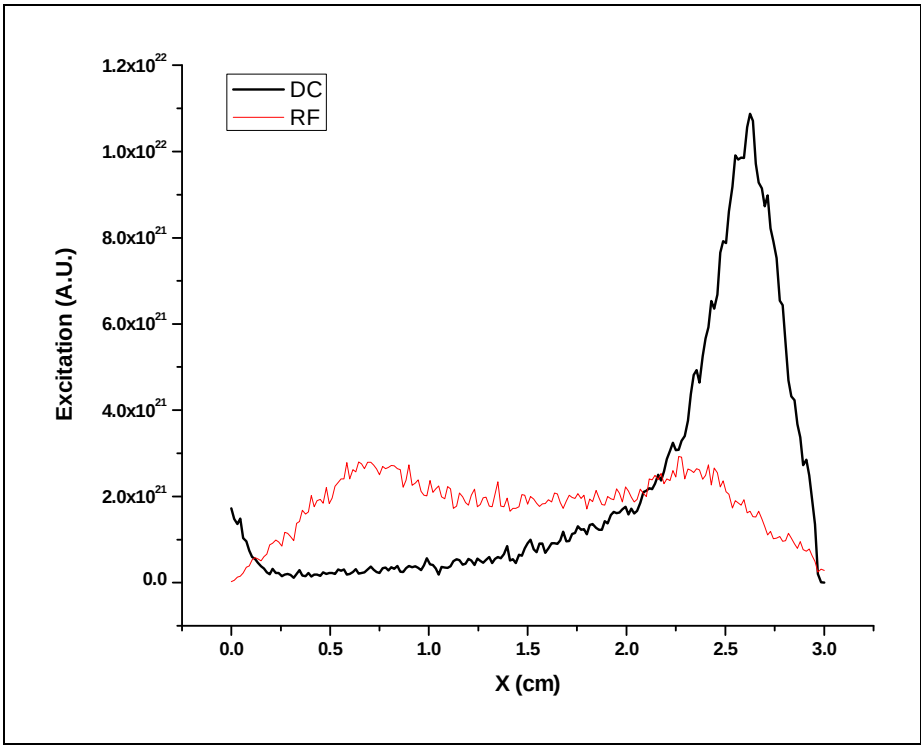

Figure 4.30: Comparison of electron-neutral excitation cross section for DC and RF discharges.

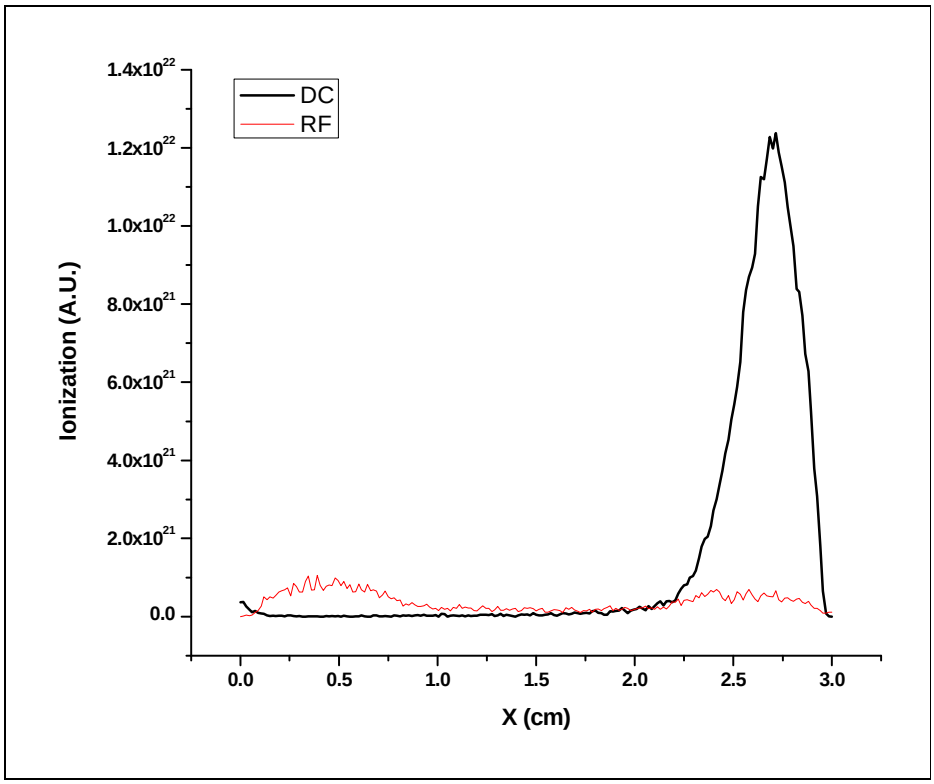

Figure 4.31: Comparison of electron-neutral ionization cross section for DC and RF discharges.

As can be seen from these results, the cross sections for the various processes are more prominent in the central region of the discharge, though the excitation and ionization cross sections are slightly higher near to the two electrodes. In comparison, the cross sections for these fundamental processes are most prominent near to the cathode.